

# RESEARCH ACTIVITIES IX

## Research Center for Molecular-Scale Nanoscience

### IX-A Nano-Science and Nano-Technology toward Molecular Scale Electronics

Molecular electronics is a fairly new and fascinating area of research that is firing the imagination of scientists. However, most single organic molecules are not conductive in a classical sense, long range electronic transport through single molecules can not be so effective to realize practical electronic circuits. Our group is interested in (1) construction of nano-structures made from conductive materials such as carbon nanotubes, metal particles or rods, with functional organic molecules, (2) measurements of electric or photonic properties of individual nano-structures while observing their nanometric images, and (3) conductance change of single molecules by external stimulation such as electric field, photon irradiation or chemical species.

#### IX-A-1 Synthesis and Self-Assembly of Novel Porphyrin Molecular Wires

**KAWAO, Masahiro<sup>1</sup>; OZAWA, Hiroaki<sup>2</sup>; TANAKA, Hirofumi<sup>3</sup>; OGAWA, Takuji<sup>3</sup>**  
(<sup>1</sup>JST and Ehime Univ.; <sup>2</sup>JST and SOKENDAI; <sup>3</sup>IMS and JST)

[*Thin Solid Films* **499**, 23–28 (2005)]

Sub-micrometer long butadiyne-linked porphyrin wires were synthesized by oxidative coupling of diethynylporphyrin. The porphyrin wires were analyzed by analytical gel permeation chromatography, absorption spectroscopy and matrix-assisted laser desorption/ionization time of flight mass spectroscopy. Observations of the wire were performed by atomic force microscopy. Self-assembled structures of the wires were observed on highly oriented pyrolytic graphite. Self-assembling features of the porphyrin wires depended on the length of the porphyrin wires and the concentration of the depositing solution.

#### IX-A-2 Molecular Junctions Composed of Oligothiophene Dithiol Bridged Gold Nanoparticles Exhibiting Photoresponsive Properties

**HUANG, Wei<sup>1</sup>; MASUDA, Gou<sup>2</sup>; MAEDA, Seisuke<sup>2</sup>; TANAKA, Hirofumi<sup>3</sup>; OGAWA, Takuji<sup>3</sup>**  
(<sup>1</sup>Nanjing Univ.; <sup>2</sup>Ehime Univ.; <sup>3</sup>IMS and JST)

[*Chem. Eur. J.* **12**, 607–619 (2005)]

Three oligothiophene dithiols with different number of thiophene rings (3, 6 or 9) were synthesized and characterized. X-ray single crystal structures of compounds 3',4'-dibutyl-5'5''-dithiocyno-2,2':5',2''-terthiophene (**2**) and 5,5''''-dithiocyno-tetrabutyl-2,2':5',2''':5''',2''''':5''''',2''''''':5''''''',2''''''''-hexathiophene (**5**) were involved herein to show the exact molecular lengths as well as the difference between their UV-vis spectra arising from the different packing modes. These dithiols with different chain lengths were then treated with *t*-dodecanethiol protected active gold nano-particles (Au-

NPs) *via* in situ thiol-to-thiol ligand exchange in the presence of 1 μm gap Au-electrodes. Thus the molecular junctions composed of self-assembled films were prepared, where oligothiophene dithiol bridged Au-NPs were attached to two electrodes by means of Au-S bonded contacts. The morphologies and *I-V* characteristics of these films were studied by SEM and AFM approaches, which suggest the thickness of the films varied within the size of one isolated Au-NPs and typical distance dependent semiconductor properties could be observed. Current-voltage (*I-V*) measurements for these devices were performed where the films served as active elements in the temperature range 6 ~ 300 K and classical Arrhenius plots and their linear fittings were carried out to give the activation energies ( $\Delta E$ ). Furthermore, preliminary studies on the photoresponsive properties of these junctions were explored at 80, 160 and 300 K, respectively. Physical and photochemical mechanisms were used to explain the possible processes. To the best of our knowledge, this is the first report where oligothiophene dithiols act as bridging units to link Au-NPs, and also the first report about functionalized Au-NPs exhibiting photo response properties in the solid state.

#### IX-A-3 Simple Preparation Method for Supramolecular Porphyrin Arrays on Mica Using Air/Water Interface

**SATO, Hirokazu<sup>1</sup>; TSUTSUMI, Osamu<sup>1</sup>; TAKEDA, Kazuyoshi<sup>1</sup>; TANAKA, Hirofumi<sup>2</sup>; OGAWA, Takuji<sup>2</sup>**  
(<sup>1</sup>Ebara Research Co.; <sup>2</sup>IMS and JST)

[*Jpn. J. Appl. Phys.* **45**, 2324–2327 (2006)]

The fabrication of supramolecular porphyrin arrays on the surface of a mica substrate is demonstrated. The supramolecular structures are prepared at the air–water interface from a dilute solution of porphyrin dimer and bidentate ligand and then transferred to mica by using the conventional Langmuir-Blodgett method. Isolated wire-like structures and networks of structures are observed by atomic force microscopy. From the analysis of the height histogram and average width, these structures are considered to be side-by-side arrangements of supramolecular chains of porphyrin dimer and bidentate

ligand. By changing the ligand molecule, we demonstrate that the configuration of the supramolecular structure can be controlled.

#### IX-A-4 Porphyrin Molecular Nanodevices Wired Using Single-Walled Carbon Nanotubes

TANAKA, Hirofumi<sup>1</sup>; YAJIMA, Takashi;  
MATSUMOTO, Takuya<sup>2</sup>; OTSUKA, Yoichi<sup>2</sup>;  
OGAWA, Takuji<sup>1</sup>  
(<sup>1</sup>IMS and JST; <sup>2</sup>Osaka Univ. and JST)

[*Adv. Mater.* **18**, 1411–1415 (2006)]

For the future development of molecular electronics, we should construct nanosized molecular devices placed on nanowiring. To obtain high-quality devices composed of a few molecules, the wiring and the device should be connected well to maintain a constant interface. For this purpose, a single-walled carbon nanotube (SWNT)/porphyrin complex was prepared and then its electronic property was investigated while observing a topographic image using point-contact current imaging atomic force microscopy (PCI-AFM). Using PCI-AFM, we can measure the current along the long axis of the wiring by which the quality of the device in the circuit can be determined. The *I-V* curves were asymmetric with respect to the origin where an aggregate of several porphyrin molecules was absorbed, while they were symmetric without them. This means the porphyrin aggregation works as a rectification device on SWNT wiring. This is the first study which proves the electron property of a few porphyrin molecules absorbed on SWNT.

#### IX-A-5 Electronic Properties of Single-Walled Carbon Nanotube/150mer-Porphyrin System Measured by Point-Contact Current Imaging Atomic Force Microscopy

TANAKA, Hirofumi<sup>1</sup>; YAJIMA, Takashi<sup>2</sup>; KAWAO, Masahiro<sup>2</sup>; OGAWA, Takuji<sup>1</sup>  
(<sup>1</sup>IMS and JST; <sup>2</sup>SOKENDAI)

[*J. Nanosci. Nanotechnol.* **6**, 1644–1648 (2006)]

The electronic properties of a porphyrin polymer wire absorbed on a single-walled carbon nanotube (SWNT) were investigated. Current-voltage (*I-V*) curves were measured simultaneously along with topographic observations using point-contact current imaging atomic force microscopy (PCI-AFM). *I-V* curves taken at the location of porphyrin polymer wire absorption were asymmetric with respect to the origin, while they were symmetric in the absence of a porphyrin polymer wire. The electron conduction mechanism of the porphyrin on the SWNT was similar to the case of SWNT/5,15-Bis(pentylporphyrinato) zinc(II) complex in our recent work.

#### IX-A-6 Preparation of Very Reactive Thiol-Protected Gold Nanoparticles: Revisiting the Brust-Schiffrin Method

ARAKI, Koiti<sup>1</sup>; MIZUGUCHI, Eisuke<sup>2</sup>; TANAKA, Hirofumi<sup>3</sup>; OGAWA, Takuji<sup>3</sup>  
(<sup>1</sup>Sao Paulo Univ.; <sup>2</sup>Ehime Univ.; <sup>3</sup>IMS and JST)

[*J. Nanosci. Nanotechnol.* **6**, 708–712 (2006)]

Metal nanoparticles have attracted great interest in nanoscience and nanotechnology because of the many possibilities envisaged by the bottom-up approach since they possess unique optical, electrical, bonding and catalytic properties. Among them, the gold clusters are the most stable and extensively studied materials, and have been proposed for applications such as in photo-electrochemical devices, drug delivery systems and chemical and immunosensors. In all these cases, the properties of the materials should be adjusted by anchoring molecular species with suitable properties on the surface. In this sense, the availability of easily functionalizable and stable starting materials is an important aspect since there is a myriad of molecular species and other materials that can be combined with for the development of new inorganic-organic hybrid nanomaterials and applications.

The higher stability and possibility to isolate a solid that can be repeatedly isolated and redissolved in common organic solvents without decomposition and the possibility to treat them just as another organic molecular species is very convenient. However, there is a drawback for the widespread use of such a thiol protected materials: the sluggishness of the functionalization reaction by substitution of the protecting species, which can take more than a day to proceed until completion. The use of conventional organic chemistry on  $\omega$ -functionalized protecting molecules is also tedious and hampers the preparation of organic-inorganic hybrid nanomaterials, for example by coordinative layer-by-layer assembly. Accordingly, we revisited the Brust-Schiffrin method envisaging the preparation of substitutionally reactive but stable enough thiol protected gold nanoparticles to isolate them as a solid.

#### IX-A-7 Spontaneous Resolution of Delta and Gamma Enantiomeric Pair of [Ru(phen)(bpy)<sub>2</sub>](PF<sub>6</sub>)<sub>2</sub> (phen = 1,10-phenanthroline, bpy = 2,2'-bipyridine) by Racemic Conglomerate Crystallization

HUANG, Wei<sup>1</sup>; OGAWA, Takuji  
(<sup>1</sup>Nanjing Univ.)

[*Polyhedron* **25**, 1379–1385 (2006)]

Spontaneous resolution study is realized for a  $\Delta$  and  $\Lambda$  enantiomeric pair of ruthenium(II) complexes obtained by racemic conglomeration from solution, crystallizing in *P4*<sub>1</sub> and *P4*<sub>3</sub> space groups. A ligand exchange reaction between phen and bpy ligands is found for these Ru(II) complexes, but racemization is accompanied which has been proved by the single-crystal structure of the product. To extend our research, counter-ion (BF<sub>4</sub><sup>-</sup>)

and 4,4'-dimethyl-2,2'-bipyridine (dmbpy) are used to synthesize similar six-coordinate Ru(II) complexes. Nevertheless, conglomerate crystallization could not be progressed in these two cases.

#### IX-A-8 Structural and Spectroscopic Characterizations of Low-Spin [Fe(4,4-dimethyl-2,2'-bipyridine)<sub>3</sub>] (NCS)<sub>2</sub>/H<sub>2</sub>O Prepared from High-Spin Iron(II) Dithiocyanate Tetrapyrindine

HUANG, Wei<sup>1</sup>; OGAWA, Takuji  
(<sup>1</sup>Nanjing Univ.)

[*J. Mol. Struct.* **785**, 21–26 (2006)]

Redetermination of the crystal structure of high-spin iron(II) dithiocyanate tetrapyrindine [Fe(py)<sub>4</sub>(NCS)<sub>2</sub>] (**1**) (pyZpyridine) at 85 and 291 K exhibits different unit cells when compared with that reported in 1967. An elongation in the compressed octahedron coordination environment around central ferrous ion is observed at low temperature, which can be verified by the DFT calculations of energy and dipole moments. **1** was then used as the Fe(II) source to synthesize [Fe(dmbpy)<sub>3</sub>](NCS)<sub>2</sub>·3H<sub>2</sub>O (**2**) (dmbpyZ4,40-dimethyl-2,20-bipyridine). The X-ray diffraction studies of **2** reveal that six Fe–N bond distances are in the range 1.959(3)–1.971(3) Å suggesting the formation of the low-spin Fe(II) complex.

#### IX-A-9 Morphology and Electric Properties of Nonathiophene/Au Nano-Composite Thin Films Formed between 1 μm Gapped Electrodes

OGAWA, Takuji<sup>1</sup>; HUANG, Wei<sup>2</sup>; TANAKA, Hirofumi<sup>1</sup>  
(<sup>1</sup>IMS and JST; <sup>2</sup>Nanjing Univ.)

[*Mol. Cryst. Liq. Cryst.* **455**, 299–303 (2006)]

A nano-composite conductive film is formed between gold electrodes by immersion of the electrode pair in a chloroform solution of nonathiophenedithiol and gold nanoparticles. The homogeneous thin film is formed over an area of 3 mm × 3 mm surrounding the 1 μm-gapped electrodes. The thickness of the film (20 nm) corresponds to 2–3 layers of the dithiol-bridged Au nanoparticles. Temperature-dependent *I*-*V* curves reveal that a thermionic mechanism dominates in the high-temperature region (>80 K), while molecular tunneling is the main transport process at lower temperatures.

#### IX-A-10 Synthesis of End-Functionalized π-Conjugated Porphyrin Oligomers

OZAWA, Hiroaki<sup>1</sup>; OGAWA, Takuji<sup>2</sup>; TANAKA, Hirofumi<sup>2</sup>  
(<sup>1</sup>SOKENDAI; <sup>2</sup>IMS and JST)

[*Tetrahedron* **62**, 4749–4755 (2006)]

4-(S-acetylthiomethyl)phenyl- and pyrenyl-functionalized π-conjugated porphyrin oligomers were syn-

thesized. The distribution of the length of the oligomers could be controlled by changing the ratio of the starting porphyrin to the capping molecules. Oligomers from dimers to heptamers were isolated using size exclusion chromatography. The spectroscopic properties of these oligomers were measured to determine the influences of the number of porphyrin units and capping molecules on the absorption and emission spectra.

#### IX-A-11 Fabrication of Nanoscale Gaps Using a Combination of Self-Assembled Monomolecular and Electron Beam Lithographic Techniques

NEGISHI, R.<sup>1,2</sup>; HASEGAWA, T.<sup>1,2</sup>; TERABE, K.<sup>1,2</sup>; AONO, M.<sup>1,2</sup>; EBIHARA, T.<sup>2</sup>; OGAWA, Takuji; TANAKA, Hirofumi  
(<sup>1</sup>ICORP, JST; <sup>2</sup>NIMS)

[*Appl. Phys. Lett.* **88**, 223111 (2006)]

We describe a new method of fabricating nanogaps using a combination of the self-assembled molecular lithographic and the electron beam lithographic techniques. The method enables us to control the size of a gap with an accuracy of ~2 nm, and design the positions, where the nanogap should be formed, in the high-resolution patterning by employing an electron beam lithography. The utility of the fabricated nanogap is demonstrated by measurement of a single electron tunneling phenomenon through the dodecanethiol-coated Au nanoparticles placed in the fabricated nanogap.

#### IX-A-12 Synthesis and Photochemical Behavior of Metalloporphyrin Complexes Containing a Photochromic Axial Ligand

TSUTSUMI, Osamu<sup>1</sup>; SATO, Hirokazu<sup>1</sup>; TAKEDA, Kazuyoshi<sup>1</sup>; OGAWA, Takuji  
(<sup>1</sup>Ebara Research Co.)

[*Thin Solid Films* **499**, 219–223 (2006)]

Metalloporphyrin complexes with a photochromic axial ligand were synthesized and photoisomerization behavior of those complexes was investigated. In this study, 3,3V-azopyridine (AZP) was used as the axial ligand. We found that the structure of the axial-coordinated complexes depended on the center metal of porphyrin. When magnesium was employed as the center metal, a 1:1 coordinated complex was obtained. On the other hand, zinc or rhodium porphyrins formed the sandwich-bonded complexes. The photoisomerization behavior also depended on the center metal of the porphyrins, and the *cis*-to-*trans* “one-way” photoisomerization of the AZP axial ligand took place in the complexes of zinc and rhodium porphyrins. The one-way isomerization may be interpreted as the results of the photoinduced electron transfer from porphyrin to AZP.

## IX-B Development of Organic Semiconductors for Molecular Thin-Film Devices

Organic light-emitting diodes (OLEDs) and organic field-effect transistors (OFETs) based on  $\pi$ -conjugated oligomers have been extensively studied as molecular thin-film devices. Organic semiconductors with low injection barriers and high mobilities are required for highly efficient OLEDs and OFETs. Radical cations or anions of an organic semiconductor have to be generated easily at the interface with an electrode (or a dielectric), and holes or electrons must move fast in the semiconducting layer. Compared with organic p-type semiconductors, organic n-type semiconductors for practical use are few and rather difficult to develop. Recently, we found that perfluorinated aromatic compounds are efficient n-type semiconductors for OLEDs and OFETs.

### IX-B-1 Synthesis and Characterization of Three Novel Perfluoro-Oligothiophenes Ranging in Length from the Trimer to the Pentamer

OSUNA, Reyes M.<sup>1</sup>; ORTIZ, Rocío P.<sup>1</sup>; DELGADO, Mari C. R.<sup>1</sup>; SAKAMOTO, Youichi; SUZUKI, Toshiyasu; HERNÁNDSZ, Víctor<sup>1</sup>; NAVARRETE, Juan T. L.<sup>1</sup>  
(<sup>1</sup>Univ. Málaga)

[*J. Phys. Chem. B* **109**, 20737–20745 (2005)]

In this article, we report on the synthesis and full characterization of three perfluorinated oligothiophenes, ranging in length from the trimer (PF-*n*T, with  $n = 3, 4, \text{ or } 5$ ). The differential pulse voltammetry (DPV) analysis of the compounds showed that they can be both oxidized and reduced (*i.e.*, they display a dual or amphoteric electrochemical behavior), with the reduction peaks positively shifted relative to those of the corresponding unsubstituted oligothiophenes. The electrochemically determined energy gaps are in agreement with those measured from the UV-vis-NIR absorption spectra in solution. The conjugational properties have been investigated by means of FT-Raman spectroscopy, both as pure solids and as dilute solutes in  $\text{CH}_2\text{Cl}_2$ , revealing that: (i)  $\pi$ -conjugation does not still reach saturation with chain length for the longest oligomer, and (ii) conformational distortions from a nearly coplanar arrangement of the successive thiophene units upon solution are not too large. DFT and TDDFT quantum chemical calculations have been performed, at the B3LYP/6-31G\*\* level, to assess information about the optimized molecular structure, equilibrium atomic charges distribution, energies and topologies of the frontier molecular orbitals (MO) around the gap, vibrational normal modes associated with the most outstanding Raman scatterings, and vertical one-electron excitations that give rise to the main optical absorptions.

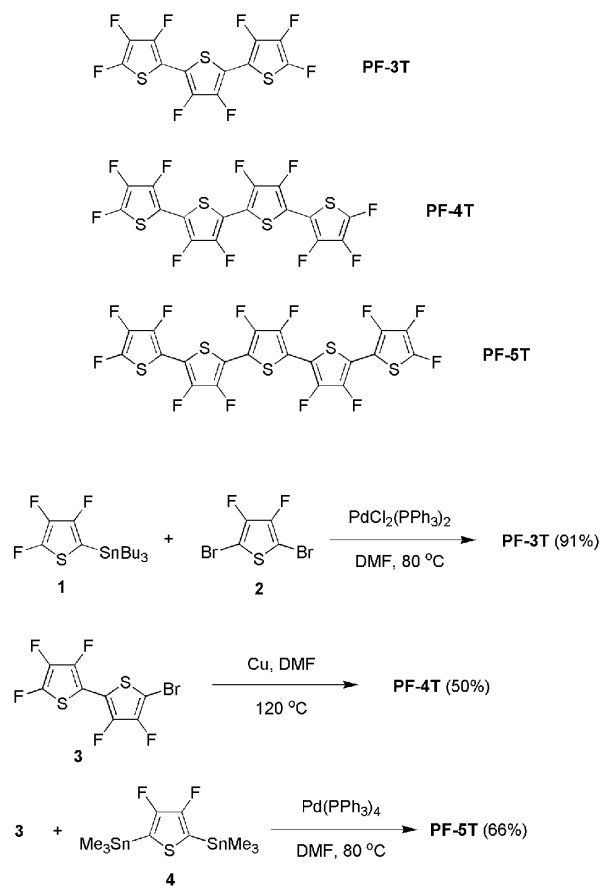


**Figure 1.** Structures and syntheses of perfluoro-oligothiophenes.

## IX-C Development of Multi-Function Integrated Macromolecules and Their Organization on Substrate Surfaces for Planar Molecular-Scale Electronics Circuits

The concept of molecular-scale electronics is now realized for individual components such as wire, diode, switch, and memory cell, but the fabrication of complete molecular-scale circuits remains challenging because of the difficulty of connecting molecular modules to one another. Molecular monolithic technology, which integrates the wiring, transistors, and the required passive elements on a single macromolecule, has been proposed as a promising solution to this problem. In this project we have been trying to establish both the architecture of this novel class of macromolecules and the protocols for their purposive organization on metal/semiconductor substrate surfaces.

### IX-C-1 Stepwise Synthesis of Molecular Wire with a Double-Tunnel Junction

TANAKA, Shoji

We have developed a synthetic protocol for precisely-defined linear macromolecules with a double-tunnel junction as shown in Figure 1. The nature of intramolecular charge transport in a  $\pi$ -conjugated macromolecule with tunnel junctions is of fundamental importance for single electron/hole device applications. In the field of applied physics metal–molecule–metal double junction systems have been intensively studied so far. In contrast, little attention has been paid to an intramolecular tunnel junction system because of the problem of precise fabrication of tunnel junction structures in a macromolecule. Based on our synthetic approach, a series of intramolecular junction systems will be prepared from various types of non-conjugated molecular blocks and the 1–10 nm long  $\pi$ -conjugated molecular blocks that we have already developed.

### IX-C-2 Direct Identification of Conformational Isomers of Adsorbed Oligothiophene on Cu(100)

YOKOYAMA, Takashi<sup>1</sup>; KURATA, Saki<sup>1</sup>; TANAKA, Shoji  
(<sup>1</sup>Yokohama City Univ.)

[*J. Phys. Chem. B* in press]

A direct conformational analysis using scanning tunneling microscopy (STM) has been performed for individual adsorbed  $\alpha$ -octithiophene molecules **8T-Si** on Cu(100). *s-Cis* and *s-trans* conformational isomers are induced by the rotational flexibility of individual thiophene rings. By adding bulky N-silyl substituents to octithiophene, we successfully identify the *s-cis* and *s-trans* conformational isomers using STM. The obtained relative abundances of the *s-cis* and *s-trans* conformations are analyzed using ab initio molecular orbital calculations.

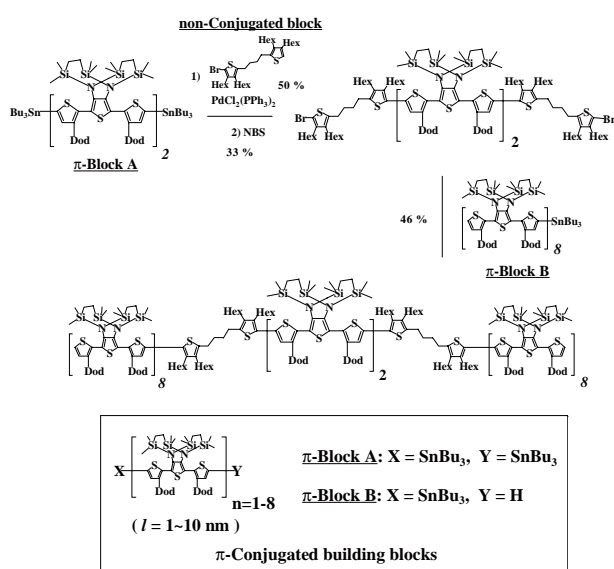


**Figure 1.** Synthetic scheme of 25 nm long molecular wire with a double-tunnel junction.

## IX-D Nano- and Complex-Catalysis

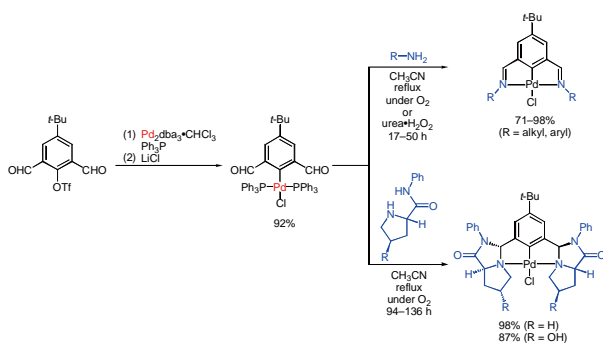
Objectives of this research group is development of nano- and complex-catalysts which exhibit novel catalytic functions, in particular, to promote efficient organic molecular transformations. Three major subjects are (1) preparation and properties of novel pincer complexes, (2) development of polymeric complex-catalysis in water, and (3) development of polymer-supported nano-metal catalysts. Representative results are shown below.

### IX-D-1 NCN Pincer Palladium Complexes: Their Preparation via a Ligand Introduction Route and Their Catalytic Properties

UOZUMI, Yasuhiro; TAKENAKA, Kazuhiro; MINAKAWA, Maki

[*J. Am. Chem. Soc.* **127**, 12273–12281 (2005)]

A wide range of NCN pincer palladium complexes, [4-*tert*-2,6-bis(*N*-alkylimino)phenyl]chloropalladium (alkyl = *n*-butyl, benzyl, cyclohexyl, *t*-butyl, adamantyl, phenyl, 4-methoxyphenyl), were readily prepared from *trans*-(4-*tert*-butyl-2,6-diformyl-phenyl)chlorobis(triphenylphosphine)palladium via dehydrative introduction of the corresponding alkylimino ligand groups (ligand introduction route) in excellent yields (71–98%). NMR studies on this route for forming pincer complexes revealed the intermediacy of [4-*tert*-2,6-bis(*N*-alkylimino)phenyl]chlorobis(triphenylphosphine)palladium which is in equilibrium with the corresponding NCN pincer complexes via coordination/dissociation of the intramolecular imino groups and triphenylphosphine ligands. A series of chiral NCN pincer complexes bearing pyrroloimidazolone units as the *trans*-chelating donor groups, [4-*tert*-butyl-2,6-bis{(3*R*,7*aS*)-2-phenylhexahydro-1*H*-pyrrolo[1,2-*c*]imidazol-1-on-3-yl}phenyl]chloropalladium, were also prepared from the same precursor via condensation with proline anilides in high yields. The catalytic properties of the NCN imino and the NCN pyrroloimidazolone pincer palladium complexes were examined in the Heck reaction and the asymmetric Michael reaction to demonstrate their high catalytic activity and high enantioselectivity.

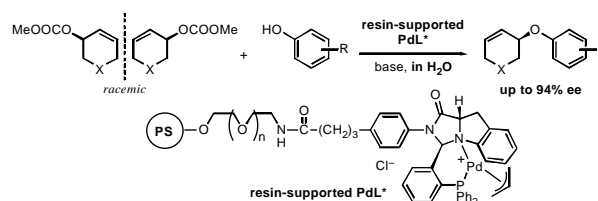


### IX-D-2 Asymmetric P-Allylic Etherification of Cycloalkenyl Esters with Phenols in Water Using a Resin-Supported Chiral Palladium Complex

UOZUMI, Yasuhiro; KIMURA, Masahiro

[*Tetrahedron:Asymmetry* **17**, 161–166 (2006)]

Catalytic asymmetric allylic amination of cycloalkenyl carbonates (methyl cyclohexen-2-yl carbonate, methyl cyclohepten-2-yl carbonate, methyl 5-methoxycarbonylcyclohexen-2-yl carbonate, methyl cyclohexenyl carbonate, *t*-butyl 5-methoxycarbonyloxy-1,2,5,6-tetrahydropyridinedicarboxylate) with phenolic nucleophiles was achieved in water under heterogeneous conditions by use of a palladium complex of (3*R*,9*aS*)-3-[2-(diphenylphosphino)phenyl]-2-phenyltetrahydro-1*H*-imidazo[1,5-*a*]indole-1-one anchored on polystyrene-poly(ethylene glycol) copolymer resin (2 mol % Pd) to give the corresponding cycloalkenylamines with high enantiomeric selectivity (up to 94% *ee*).

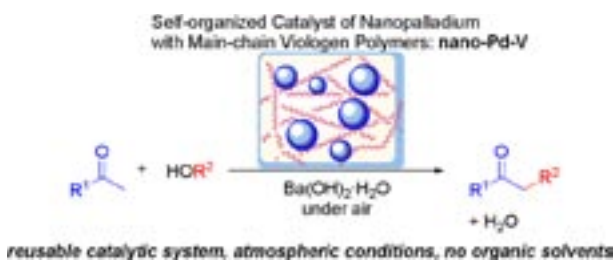


### IX-D-3 A Solid-Phase Self-Organized Catalyst of Nanopalladium with Main-Chain Viologen Polymers: $\alpha$ -Alkylation of Ketones with Primary Alcohols

YAMADA, Yoichi; UOZUMI, Yasuhiro

[*Org. Lett.* **8**, 1375–1378 (2006)]

A novel solid-phase self-organized catalyst of palladium nanoparticles was prepared from PdCl<sub>2</sub> with main-chain viologen polymers via complexation and reduction. This insoluble nanocatalyst nano-Pd-V efficiently promoted  $\alpha$ -alkylation of ketones with primary alcohols in the presence of Ba(OH)<sub>2</sub>·H<sub>2</sub>O under atmospheric conditions without organic solvents. The nano-Pd-V catalyst was reused without loss of catalytic activity.



## IX-E Development of New Nanomaterials as Components in Advanced Molecular Systems

Nanometer-sized materials exhibit unique electronic behavior. In the quest of advanced redox catalysis, we are currently interested in combining nanometer-sized materials into molecular redox systems. As a basic architecture, composites of organic molecules and gold nanoparticles were synthesized and molecular dynamic simulations were carried out to predict the solution structures.

### IX-E-1 Automated Design of Protecting Molecules for Metal Nanoparticles by Combinatorial Molecular Simulations

NAGATA, Toshi

[*J. Organomet. Chem.* in press]

New tripod oligo(dibenzyl sulfide) molecules were designed by computer modeling calculations so that they would form 1:1 complexes with an Au<sub>147</sub> nanoparticle. Twelve aromatic molecules containing two methylthiomethyl groups were used as construction units ("residues"). Combinations of the residues ("sequences") were examined by molecular dynamic simulations, and those sequences giving the largest interaction energies with the gold nanoparticle were sought through either full search or genetic algorithm. Best-fit sequences were found for  $N = 5$  and 6 ( $N$  is the number of "residues" in one leg of the tripod molecule).

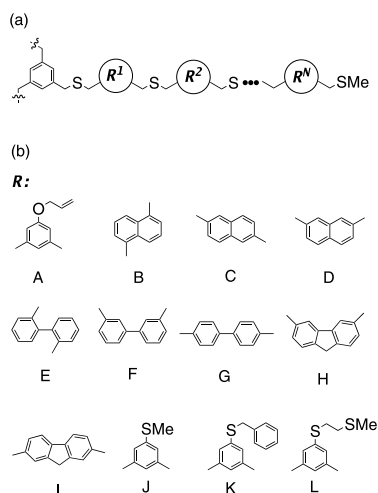


**Figure 1.** (a) The base structure of the protecting molecule. (b) The "residues" used in this study.

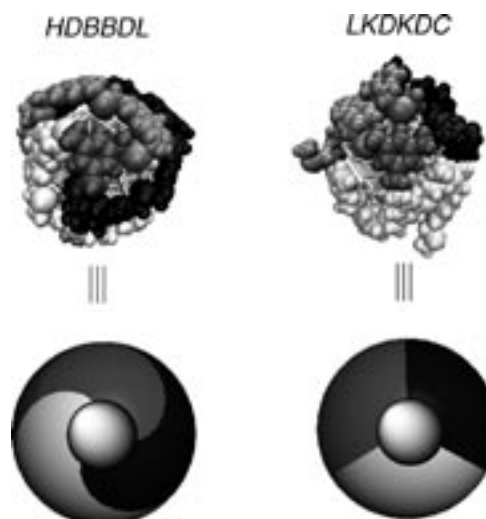


**Figure 2.** The surface covering schemes for the two lowest energy structures for  $N = 6$ . The atoms in the three "legs" are drawn in white, gray, and black, respectively.

## IX-F Designing Artificial Photosynthesis at Molecular Dimensions

Photosynthesis is one of the finest piece of molecular machinery that Nature has ever created. Its ultrafast electron transfer and following well-organized sequence of chemical transformation have been, and will continue to be, challenging goals for molecular scientists. Our ultimate goal is to design artificial molecular systems that effect multiple chemical reactions triggered by light on the basis of molecular rationale.

### IX-F-1 Elucidation of Solution Structures of Dendrimer-Linked Porphyrins

KIKUZAWA, Yoshihiro; NAGATA, Toshi; TAHARA, Tahei<sup>1</sup>; ISHII, Kunihiko<sup>1</sup>  
(<sup>1</sup>RIKEN)

[Chem. Asian J. in press]

In order to estimate the average structures of our ferrocene-dendrimer-porphyrins (Figure 1), we carried molecular-dynamic (MD) simulations of these molecules in  $\text{CHCl}_3$  solutions. Figure 2 shows the spatial distribution of the iron atoms of all the ferrocenyl groups, in relative to the porphyrin ring at the core. Figure 3 shows the radial distribution functions of the iron atoms in the first, second, and third layers from the center of the porphyrin ring. These figures clearly show that only the ferrocenyl groups in the second layer have significant probability to approach the porphyrin ring closer than 10 Å. This observation is consistent with the results of <sup>1</sup>H NMR and fluorescence quenching, namely the second layer had a larger interaction with the porphyrin ring than the first and third layers.

It is also interesting to note that such layered distribution was more distinct in  $\text{G3}(\text{Fc})_{14}\text{-ZnP}$  than in  $\text{G2}(\text{Fc})_6\text{-ZnP}$ , the generation 2 compound with the similar architecture. The spatial distribution and radial distribution functions of the iron atoms in  $\text{G2}(\text{Fc})_6\text{-ZnP}$  also showed similar trends as  $\text{G3}(\text{Fc})_{14}\text{-ZnP}$ , although the distribution of the first layer Fe atoms was somewhat broader in  $\text{G2}(\text{Fc})_6\text{-ZnP}$  than in  $\text{G3}(\text{Fc})_{14}\text{-ZnP}$ . These results suggest that, even in the case of these “spatially relaxed” dendritic frameworks, the presence of the higher-generation branches restricts the movements of the inner layer.

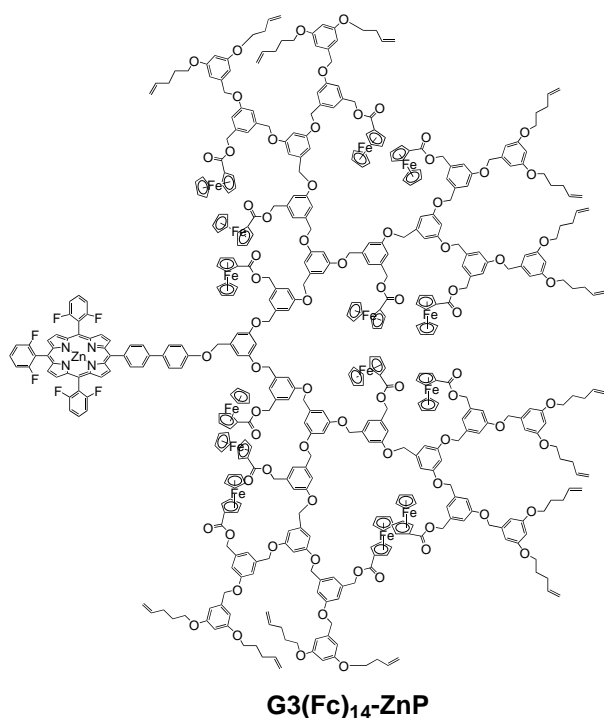


**Figure 1.** The structure of the ferrocene-dendrimer-linked porphyrin (generation 3).

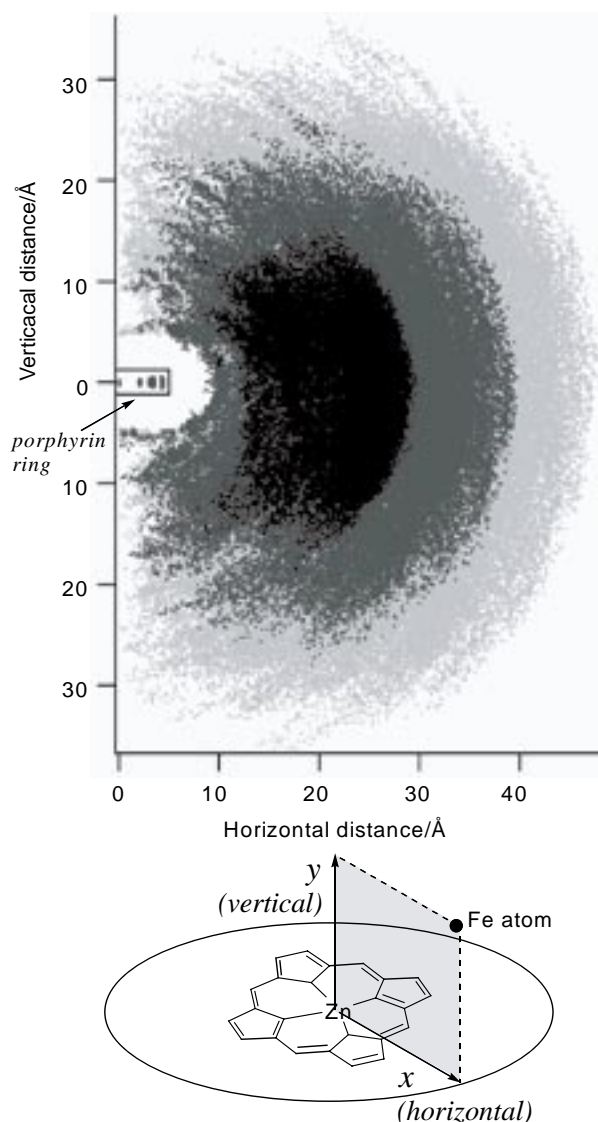


**Figure 2.** The calculated distribution of the iron atoms of the ferrocenyl groups in  $\text{G3}(\text{Fc})_{14}\text{-ZnP}$ . The first, second, and third layer are represented by dark gray, medium gray, and light gray respectively.

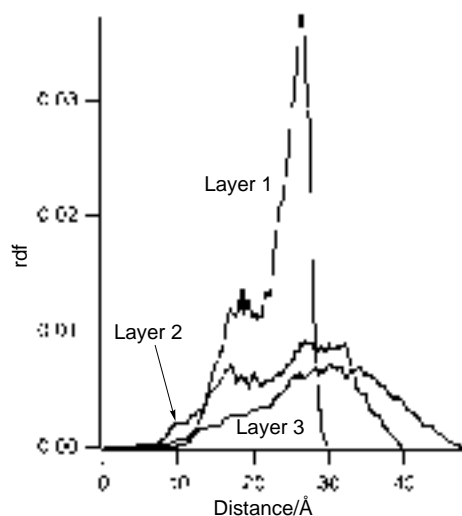


**Figure 3.** Radial distribution function (per single atom) of the iron atoms in each layer in  $\text{G3}(\text{Fc})_{14}\text{-ZnP}$ .

### IX-F-2 Reconstitution of the Water-Oxidizing Complex in Manganese-Depleted Photosystem II Preparations Using Binuclear Mn(II) and Mn(IV) Complexes

NAGATA, Toshi; NAGASAWA, Takayuki;  
ZHARMUKHAMEDOV, Sergei K.<sup>1</sup>;  
ALLAKHVERDIEV, Suleyman I.<sup>2</sup>

(<sup>1</sup>Inst. Basic Biological Problems, Russian Acad. Sci.;  
<sup>2</sup>IMS and Inst. Basic Biological Problems, Russian Acad. Sci.)

Reconstitution of the Mn-depleted Photosystem II (PSII) particles with synthetic binuclear Mn complexes (two Mn(II)<sub>2</sub> complexes and one Mn(IV)<sub>2</sub> complex) was examined. The reconstituted PSII particles showed lower restored activities than our previous studies in photo-induced electron transfer and oxygen evolution. These results were ascribed to the "robustness" of the Mn complexes used in this study. The ESI-MS spectra of the Mn(II)<sub>2</sub> complexes showed that the macrocyclic ligand remained intact even after release of the Mn(II) ions, so it was proposed that the macrocyclic ligand remained in the vicinity of the PSII proteins and caused distortion of the protein structures. On the other hand, the lower activity of the Mn(IV)<sub>2</sub> complex was ascribed to the robustness of the bis- $\mu$ -oxo structure which caused transfer of the Mn ions to the PSII protein less efficient than the previously examined Mn complexes with mono-nuclear or mono- $\mu$ -oxo binuclear structures. These results implies that subtle balance between the stability and lability of the complexes are important in successful reconstitution of PSII.

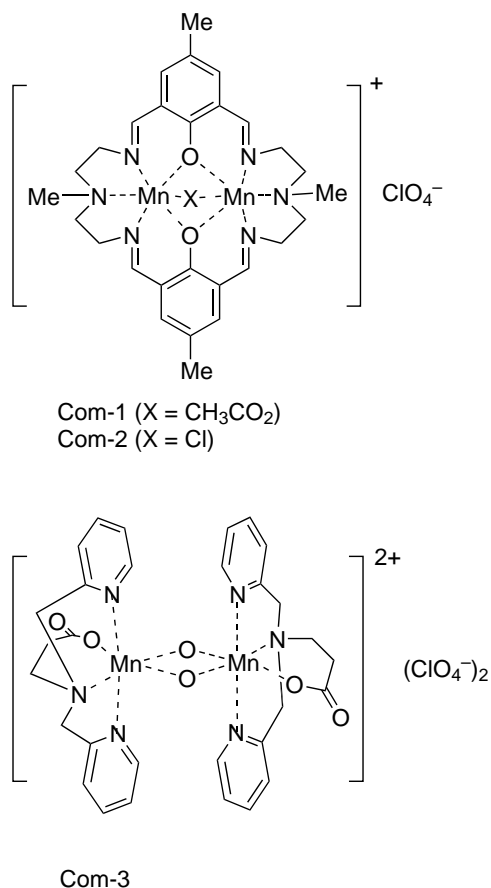


**Figure 1.** The structures of the synthetic dimanganese complexes.

## IX-G Development of New Metal Complexes as Redox Catalysts

Redox catalysis is an important field of chemistry which translates a flow of electron into chemical transformation. It is also one of the requisites for artificial photosynthesis. This project of ours aims at developing new metal complexes that perform redox catalysis at low overpotential. Currently we are focusing our attention to the development of a series of cobalt phosphine complexes as possible catalysts for electrochemical reductions.

### IX-G-1 Syntheses and Structures of Co(I) Complexes Having Cyclopentadienyl Auxiliaries and C-P Bond Cleavage of the Coordinated Phosphine

NAGASAWA, Takayuki; NAGATA, Toshi

The strong basicity of low-valent cobalt complexes are attractive in electrocatalytic organometallic chemistry. Here we report the syntheses and molecular structures of Co(I) complexes with cyclopentadienyl derivatives and an unexpected cleavage of a C-P bond in triphenylphosphine by Co(I) under mild conditions.

Reactions of ClCo(PPh<sub>3</sub>)<sub>3</sub> with sodium salts of cyclopentadienyl derivatives NaCp<sup>R</sup> (R = H, COOMe, CH<sub>2</sub>CH<sub>2</sub>SMe) gave five-coordinate Co(I) complexes

Cp<sup>R</sup>Co(PPh<sub>3</sub>)<sub>2</sub> (R = H, **2**; COOMe, **3**; CH<sub>2</sub>CH<sub>2</sub>SMe, **4**) in 60–80% yields as crystals. The structures of **2–4** were determined by X-ray crystallography (Figure 1).

On the other hand, the reaction of LiCp\* (Cp\* = C<sub>5</sub>Me<sub>5</sub>) with ClCo(PPh<sub>3</sub>)<sub>3</sub> resulted in a formation of a diamagnetic dimer complex [Cp\*Co(μ-Ph)(μ-PPh<sub>2</sub>)CoCp\*], **5**, which has bridging phenyl and diphenylphosphide groups. This compound was isolated from hexane solution as black crystals in 64% yield. The structure was confirmed by X-ray crystallography (Figure 2). We propose that the bridging phenyl and phosphide ligands were generated by a C-P bond cleavage caused by the action of the strongly nucleophilic Cp\*Co fragment.

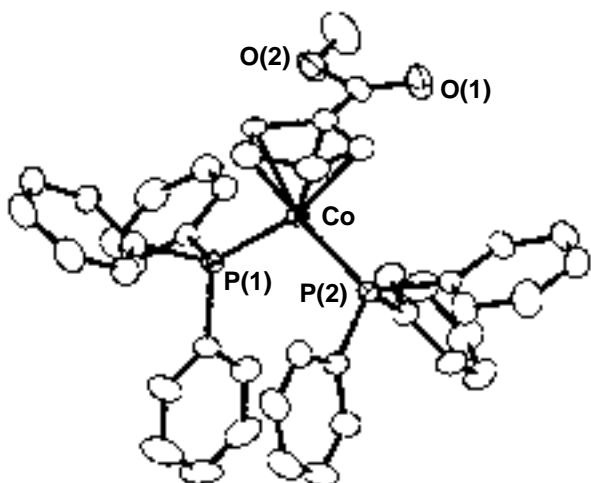


Figure 1. The ORTEP drawing of 3.

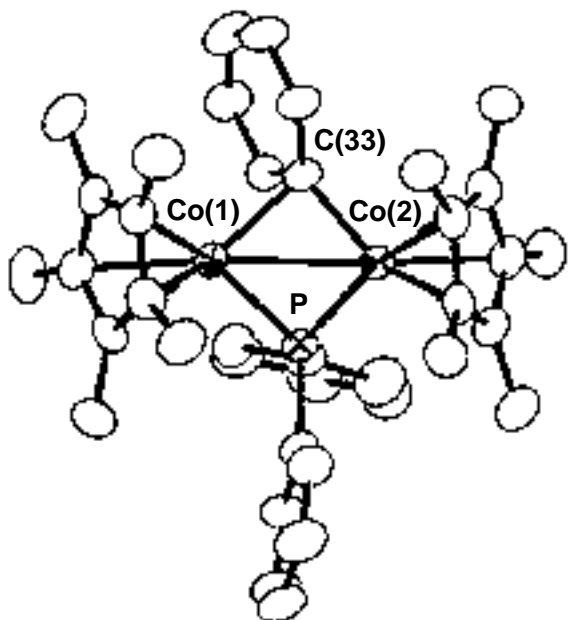


Figure 2. The ORTEP drawing of 5.

## IX-H Synthesis of Buckybowls and Heterobuckybowls

Bowl-shaped  $\pi$ -conjugated compounds including partial structures of the fullerenes, which are called "buckybowls," are of importance not only as model compounds of fullerenes but also as their own chemical and physical properties. Heteroatom-containing buckybowls (heterobuckybowls) have also been expected to exhibit unique physical characters. For example, in solution they show the characteristic dynamic behavior such as bowl-to-bowl inversion. On the other hand, they sometimes favor stacking structure in a concave-convex fashion in the solid state, giving excellent electron conductivity. Furthermore, some buckybowls are conceivable to possess the bowl-chirality if the racemization process, as equal as bowl-to-bowl inversion, is slow enough to be isolated. However, very few buckybowls/heterobuckybowls has been achieved for preparation mainly due to their strained structure, and no report on the preparation of chiralbowls has appeared. In addition, most of thus-reported procedures are performed under severe reaction conditions, limiting the sort of the introducible atoms/functional groups.

In the present project, we develop the rational route to the various kinds of buckybowls/heterobuckybowls using the organic synthesis approach.

### IX-H-1 Regio- and Stereo-Selective Synthesis of Multi-Substituted Benzene Derivatives by Cyclotrimerization of Haloalkene Derivatives

**SAKURAI, Hidehiro; HIGASHIBAYASHI, Shuhei**

Bridged multi-substituted benzene derivatives have been of interest because of the bond alternation of benzene ring and the utility for syntheses of cup-shaped molecules or buckybowls. The regio- and stereo-selective syntheses are important for the synthetic utility. Chiral multi-substituted benzene derivatives were synthesized from chiral halonorbornene derivatives through the regio- and stereo-selective cyclotrimerization catalyzed by palladium nanocluster. Thus prepared chiral benzene derivatives are expected to serve as the synthetic intermediates for chiral buckybowls.

## IX-I Spectroscopy and Chemistry of Metal Nanoclusters on Surfaces

The structure and reactivity of metal nanoclusters are important issues because of their relevance to heterogeneous catalysis. In particular, Au nanoclusters on titanium oxide surfaces has attracted a lot of interest since the discovery of its catalytic activity on CO oxidation. We apply various surface science techniques to clarify correlations between structures and reactivity of metal nanoclusters deposited on surfaces. In this year, we use alkanethiolate-coated gold nanoclusters as a primary target in collaboration with Tsukuda (IMS) and Al-Shamery (U. Oldenburg) groups.

### IX-I-1 STM Observation and Fabrication of Films of Gold Nanoclusters with and without Alkanethiolate Ligands on TiO<sub>2</sub>(110)

**MATSUMOTO, Taketoshi; NICKUT, Patricia<sup>1</sup>; SAWADA, Takeshi; TSUNOYAMA, Hironori; WATANABE, Kazuya; TSUKUDA, Tatsuya; AL-SHAMERY, Katharina<sup>1</sup>; MATSUMOTO, Yoshiyasu**  
(<sup>1</sup>Carl v. Ossietzky U. Oldenburg)

Films of Au nanoclusters protected with alkanethiolate ligands fabricated before and after etching on the TiO<sub>2</sub>(110) surface were investigated by scanning tunneling microscopy (STM) and X-ray photoelectron spectroscopy (XPS). The Au nanoclusters were produced by reducing HAuCl<sub>4</sub> in micelles and fractionalized by

size with gel permeation chromatography. Au nanoclusters with hexanethiolate formed single layers and were coated on TiO<sub>2</sub>(110). Replacing the ligands with *n*-octadecanethiolate resulted in forming three layers. Au nanoclusters with ligands are mobile on TiO<sub>2</sub> at room temperature and it is possible to manipulate their positions by a STM tip. XPS spectra showed that O-atom etching removes ligands effectively and produces gold oxide on nanocluster surfaces. The oxide was reduced effectively by H atom etching. These etching procedures causes aggregation of Au nanoclusters, increasing apparent height from ~1.5 nm to 3–6 nm. Adding hexanethiol and decane to the films of Au nanocluster with hexanethiolate did not show significant changes before and after etching. No diffusion was induced by STM tips after O atom etching.

## IX-J Photochemistry on Well-Defined Surfaces

Upon the irradiation of light in the wavelength range from visible to ultraviolet, a number of adsorbed molecules on metal surfaces reveal variety of photochemical processes, including photo-stimulated desorption, rearrangement of adsorbed states, photodissociation, and photo-initiated reactions with coadsorbates. A central and fundamental question in the surface photochemistry is to clarify how adsorbate-substrate systems are excited by photon irradiation. In addition, since photo-initiated reactions can be induced without any thermal activation of reactants, they may provide good opportunities for studying a new class of surface reactions that may not be induced thermally. We have studied photochemistry of various adsorption systems on well-defined metal and semiconductor surfaces mainly by temperature-programmed desorption (TPD), infrared reflection absorption spectroscopy (IRAS), x-ray photoelectron spectroscopy (XPS), work function measurements, and angular-resolved time-of-flight (TOF) mass spectrometry of photodesorbed species associated with pulsed laser irradiation. In this year, the photochemistry of cyclic alkane on Pt(111) and Cu(111) surfaces was studied mainly by TPD, XPS, and IRAS.

### IX-J-1 Photochemistry of Cyclohexane on Cu(111)

**YAMAGUCHI, Dai; MATSUMOTO, Taketoshi; WATANABE, Kazuya; TAKAGI, Noriaki<sup>1</sup>; MATSUMOTO, Yoshiyasu**  
(<sup>1</sup>SOKENDAI and Univ. Tokyo)

[*Phys. Chem. Chem. Phys.* **8**, 179–185 (2006)]

The photochemistry of cyclohexane on Cu(111) and its excitation mechanism have been studied by temperature-programmed desorption, ultraviolet and X-ray photoelectron spectroscopy. Cyclohexane weakly adsorbed on Cu(111) has been known to show a broadened

and redshifted CH stretching band, *i.e.*, CH vibrational mode softening. Although no dehydrogenation takes place thermally on this surface and by the irradiation of photons at 5.0 eV, adsorbed cyclohexane is dissociated to cyclohexyl and hydrogen by the irradiation of photons at 6.4 eV. This is a marked contrast to cyclohexane in the gas phase where the onset of absorption is located at 7 eV. When the surface irradiated by 6.4-eV photons is further annealed, cyclohexyl is dehydrogenated to form cyclohexene that desorbs at 230 K. The systematic measurements of photochemical cross sections at 6.4 eV with linearly polarized light as a function of incident angle indicate that the electronic transition from the highest occupied band of cyclohexane to a partially occupied hybridized band near the Fermi level is respon-

sible for the photochemistry. The hybridized band is formed by the interactions between the electronic states of cyclohexane and the metal substrate. The role of the hybridized band in the photochemistry and the CH vibrational mode softening is discussed.

### IX-J-2 Photochemistry and Post-Irradiation Chemistry of Cyclohexane on Pt(111)

**YAMAGUCHI, Dai; MATSUMOTO, Taketoshi; WATANABE, Kazuya; TAKAGI, Noriaki<sup>1</sup>; MATSUMOTO, Yoshiyasu**  
(<sup>1</sup>SOKENDAI and Univ. Tokyo)

Photochemistry and post-irradiation thermal chemistry of cyclohexane on Pt(111) were investigated by TPD, XPS and IRAS. From TPD results, photo-dehydrogenation of cyclohexane was confirmed on Pt(111). IRAS spectra after photo-irradiation indicate that the primary photoproduct is cyclohexyl. The photoreaction cross sections of cyclohexane on Pt(111) at 6.4 and 5.0 eV are  $(3.1 \pm 0.2) \times 10^{-21}$  and  $(1.1 \pm 0.6) \times 10^{-21}$  cm<sup>2</sup>, respectively. The appreciable cross section at 5.0 eV suggests the larger adsorbate interactions on Pt(111)

compared with those on Cu(111). The excitation mechanism was investigated by the same procedure for Cu(111). The cross sections with p-polarized light again deviate from the absorbance of the substrate. This indicates clearly that the excitation mechanism is the same on Cu(111). On Pt(111), it has been known that cyclohexane is thermally dehydrogenated to benzene *via* C<sub>6</sub>H<sub>9</sub>. Benzene converted from the monolayer of cyclohexane does not desorb molecularly because benzene is further dehydrogenated to atomic C. In contrast, after photo-irradiation at 6.4 eV, the desorption of benzene in post-irradiation TPD was clearly observed. Then, the thermal reactions of the primary photoproduct, cyclohexyl, were investigated by IRAS. Absorption bands attributable to cyclohexene appeared at 200 K. This species has not been identified in the studies on thermal reactions of cyclohexane on Pt(111). UV photons can produce a larger amount of cyclohexyl than that induced thermally. In this case, the adsorption sites are largely occupied by produced cyclohexyl and hydrogen, which may increase the activation barriers for dehydrogenation of cyclohexene and benzene in the post-irradiation thermal chemistry.

## IX-K Ultrafast Dynamics at Well-Defined Surfaces

To understand the mechanism of surface photochemistry, it is vital to know how photoinduced electronic excitation induces adsorbate nuclear motions that ultimately lead to chemical reactions. We demonstrate the real-time observations of surface phonons and adsorbate-substrate vibrational modes by fs time-resolved second harmonics generation (TRSHG). If an excitation light pulse has a duration sufficiently shorter than a period of a vibrational mode or a phonon mode, it can excite the mode with a high degree of temporal and spatial coherence. This coherent nuclear motion modulates the second-order susceptibility  $\chi^{(2)}$ . Thus, by monitoring the intensity modulation of the second harmonics (SH) generation of a probe pulse, we can observe the evolution of the coherent nuclear motion subsequent to the electronic excitation at the surfaces. This year, in particular, we have focused on K on Pt(111) and Na on Cu(111) adsorption systems.

### IX-K-1 Coherent Surface Phonon Dynamics at K-Covered Pt(111) Surfaces Investigated by Time-Resolved Second Harmonic Generation

**FUYUKI, Masanori<sup>1</sup>; WATANABE, Kazuya; MATSUMOTO, Yoshiyasu**  
(<sup>1</sup>SOKENDAI)

[Phys. Rev. B submitted]

We have investigated coherently excited surface phonons at K-covered Pt(111) surfaces by using femto-second time-resolved second harmonic generation spectroscopy. The frequency of the K–Pt stretching phonon mode depends on the superstructure of K: 5.0–5.3 and 4.5–4.8 THz for (2×2) and  $(\sqrt{3} \times \sqrt{3})R30^\circ$  superstructures, respectively. In addition to the stretching mode, a couple of Pt surface phonon modes are simultaneously observed when the  $(\sqrt{3} \times \sqrt{3})R30^\circ$  superstructure is formed. The dephasing time of the K–Pt stretching mode becomes shorter and its frequency redshifts as the absorbed fluence of a pump pulse increases. This is

in stark contrast to the Pt surface phonon modes whose frequencies are independent of fluence. The fluence dependence of the K–Pt stretching mode is interpreted to be due to anharmonic coupling between the K–Pt stretching and lateral modes.

### IX-K-2 Excitation Mechanism of Coherent Surface Phonons on Na-Covered Cu(111)

**FUYUKI, Masanori<sup>1</sup>; WATANABE, Kazuya; INO, Daisuke<sup>1</sup>; MATSUMOTO, Yoshiyasu**  
(<sup>1</sup>SOKENDAI)

We observed time-resolved second harmonic signals from the Cu(111) surface with a full monolayer of Na in ultra-high vacuum and investigated the excitation-wavelength dependence of the wave packet dynamics of the coherently excited Na–Cu stretching mode. Changing the photon energy of the pump pulse (25 fs) from 2.0 to 2.5 eV, the oscillation amplitude derived from the Na–Cu stretching motion is enhanced. The careful measurements of photon-energy dependence indicates that the

excitation efficiency mimics the absorbance of bulk Cu. Holes created in the d-bands by the optical transitions could be filled by electrons in the adsorbate-induced occupied state of the metallic quantum well by an Auger-type transition. Hence, holes can be created in the adsorbate-induced occupied state. Moreover, since this Auger decay can occur significantly faster than the oscillation period of the Na–Cu stretching mode, the substrate excitation may be a possible excitation mechanism for the coherent oscillation.

### IX-K-3 Electron Transfer Dynamics from Organic Adsorbate to a Semiconductor Surface: Zinc-Phthalocyanine on TiO<sub>2</sub>(110)

INO, Daisuke<sup>1</sup>; WATANABE, Kazuya; TAKAGI, Noriaki<sup>2</sup>; MATSUMOTO, Yoshiyasu  
(<sup>1</sup>SOKENDAI; <sup>2</sup>Univ. Tokyo)

[*J. Phys. Chem. B* **109**, 18018–18024 (2005)]

The femtosecond time-evolutions of excited states in zinc-phthalocyanine (ZnPC) films and at the interface with TiO<sub>2</sub>(110) have been studied by using time-resolved two-photon photoelectron spectroscopy (TR-2PPE). The excited states are prepared in the first singlet

excited state (S<sub>1</sub>) with excess vibrational energy. Two different films are examined: ultrathin (monolayer) and thick films of ~30 Å in thickness. The decay behavior depends on the thickness of the film. In the case of the thick film, TR-2PPE spectra are dominated by the signals from ZnPC in the film. The excited states decay with  $\tau = 118$  fs mainly by intramolecular vibrational relaxation. After the excited states cascaded down to near the bottom of the S<sub>1</sub> manifold, they decay slowly ( $\tau = 56$  ps) although the states are located at above the conduction band minimum of the bulk TiO<sub>2</sub>. The exciton migration in the thick film is the rate determining step for the electron transfer from the film to the bulk TiO<sub>2</sub>. In the case of the ultrathin film, the contribution of electron transfer is more evident. The excited states decay faster than those in the thick film, because the electron transfer competes with the intramolecular relaxation processes. The electronic coupling with empty bands in the conduction band of TiO<sub>2</sub> plays an important role in the electron transfer. The lower limit of the electron transfer rate was estimated to be 1/296 fs<sup>-1</sup>. After the excited states relax to the states whose energy is below the conduction band minimum of TiO<sub>2</sub>, they decay much slowly because the electron transfer channel is not available for these states.

## IX-L Vibrational Dynamics at Surfaces and Interfaces Studied by Time-Resolved Sum Frequency Spectroscopy

In addition to time-resolved second harmonic generation and two-photon photoemission spectroscopy, we have developed fs time-resolved sum frequency generation (SFG) spectroscopy to study ultrafast surface dynamics. Time-resolved SFG is a versatile tool for investigating vibrational dynamics at surfaces and interfaces. In this year, we applied this technique to probe vibrational energy transfer at the interface between Pt(111) and ice layers where CO monolayer is inserted.

### IX-L-1 Vibrational Energy Relaxation at the Interface of Ice/CO/Pt(111) Studied by fs Time-Resolved Sum Frequency Generation

NAGAO, Masashi; WATANABE, Kazuya; MATSUMOTO, Yoshiyasu

We studied the vibrational excitation and relaxation dynamics of surface adsorbate for D<sub>2</sub>O/CO/Pt(111) by the femtosecond time resolved vibrational SFG spectroscopy (VIS: 800 nm, 3 ps; IR: 3–5 μm, 130 fs; pump: 400 nm, 130 fs) under ultra vacuum condition. D<sub>2</sub>O/CO/Pt(111) was prepared by dosing D<sub>2</sub>O molecules on the CO covered Pt(111) surface at 140 K. Two peaks were observed in CO stretching region at 2068 and 2095 cm<sup>-1</sup> when 10 ML D<sub>2</sub>O layer was formed on the surface, because D<sub>2</sub>O crystals exhibit island growth on this surface. The former peak (ν\*(CO)) is assigned to the adsorbed CO intact with D<sub>2</sub>O and the latter (ν(CO)) is assigned to the CO free from D<sub>2</sub>O. Both peaks were

redshifted and broadened by the irradiation of a pump pulse, because the frustrated translation and rotation modes of CO coupled to Pt hot electrons generated by the excitation pulse. We found the following features in the transient SFG spectra. The maximum peak shift of ν\*(CO) was larger than that of ν(CO) and the peak shift of ν\*(CO) shows much faster recovery than that of ν(CO) within 3 ps after the excitation. We analyze the spectra by the numerical simulation of SFG polarization based on the Bloch equations, which describe the time-dependent evolution of the density matrix for the CO stretching mode. The transient response of time-resolved SFG spectra can be characterized by the time dependent adsorbate temperature, where the key parameter is the time scale on which energy flows between substrate electrons and the CO frustrated mode, τ<sub>e</sub>. To reproduce the experimental data, coupling times of τ<sub>e</sub> = 0.8 ps and τ<sub>e</sub> = 1.6 ps for ν\*(CO) and ν(CO), respectively, are required, indicating that the ν\*(CO) mode couples to the substrate hot electrons more effectively than ν(CO).

## IX-M Chemistry of One-Dimensional Nano-Surface Compounds Studied by Scanning Tunneling Microscopy

The fluctuating configurations of low-dimensional structures can be thermodynamically favorable at finite temperatures, because the energy gain overcomes the energy cost that accompanies local structural fluctuation. In particular, one-dimensional (1D) systems have a propensity to be sensitive to these fluctuations as described by one of the maxims of condensed matter physics, *i.e.*, one chain does not make a crystal. Thus, the dynamical formation of active species and sites by these fluctuations is a key factor in establishing a microscopic model for chemical reactions at surfaces and nano-structured compounds.

### IX-M-1 Direct Observation of a Propagating Chemical Wave in Disproportionation Reactions of Water on Oxidized Ag(110) Surface by Scanning Tunneling Microscopy

NAKAGOE, Osamu<sup>1</sup>; TAKAGI, Noriaki<sup>2</sup>;  
WATANABE, Kazuya; MATSUMOTO, Yoshiyasu  
(<sup>1</sup>SOKENDAI; <sup>2</sup>Univ. Tokyo)

[*J. Phys. Chem. B* submitted]

It is well known that the adsorption of O on Ag(110) results in the formation of quasi-1D structures, AgO chains, accompanied by the mass transfer of substrate atoms. AgO chains arrange periodically to form ( $n \times 1$ ) ( $n = 2 \sim 7$ ) depending on the fractional O coverage due to repulsive inter-chain interactions. On the added-row reconstructed Ag(110)( $n \times 1$ )-O surfaces, one-dimensional -Ag-O-Ag-O- chains arrange periodically. Scanning tunneling microscopy was used for studying spatio-temporal evolution of the disproportionation reaction of H<sub>2</sub>O with O adatoms on oxidized Ag(110) surfaces where quasi-one dimensional AgO chains form ordered structures. Initially the reaction takes place slowly on Ag(110)-(5 $\times$ 1)O at the end of AgO chain, whereas the reaction accelerates explosively upon the appearance of a chemical wave that propagates along the direction perpendicular to the chain. The surface morphology of the region swept over by the chemical wave completely changes from (5 $\times$ 1)-O to that with many rectangular islands, indicating the formation of H<sub>2</sub>O(OH)<sub>2</sub>. The induction time and explosive acceleration with the propagating chemical wave imply that the reaction is autocatalytic. Water clusters hydrating OH produced likely play a central role in serving as a reservoir of H<sub>2</sub>O to feed to the reaction and enhancing the reactivity of H<sub>2</sub>O with O adatoms in AgO chains.

## IX-N Structures, Stabilities and Physicochemical Properties of Organometallic Hybrid Clusters

Recently, metal clusters have gained much attention because they exhibit novel physicochemical properties that are beyond the prediction made by a dimensional scaling of those of the corresponding bulk. In this regard, metal clusters protected by thiolates or stabilized by polymers are promising candidates for elementary units of nano-scale devices. Our interests are focused on the following issues on the organometallic hybrid clusters: (1) a large-scale preparation of the subnanometer-sized clusters, (2) development of size-selection method, (3) determination of chemical compositions of size-selected clusters (*i.e.* the numbers of metal atoms and organic molecules), and (4) elucidation of effect of the core size, core shape, and interaction with organic molecules on stabilities, electronic structures, and chemical properties.

### IX-N-1 Aerobic Oxidation Catalyzed by Gold Nanoclusters as *quasi*-Homogeneous Catalysts: Generation of Hydrogen Peroxide Using Ammonium Formate

SAKURAI, Hidehiro; TSUNOYAMA, Hironori; TSUKUDA, Tatsuya

[*Trans. Mater. Res. Soc. Jpn.* **31**, 521–524 (2006)]

Gold(0) nanocluster with  $d_{av} = 1.3 \pm 0.3$  nm stabilized by poly(*N*-vinyl-2-pyrrolidone) (Au:PVP-1) showed high catalytic activity toward the generation of hydrogen peroxide in water under ambient conditions using ammonium formate as a reductant. Generation of hydrogen peroxide was monitored by tracking the conversion of *o*-tolylboronic acid to *o*-cresol. In the presence of excess ammonium formate, *o*-cresol was obtained from *o*-tolylboronic acid with ~60% yield within 24 hours at 300 K. In order to investigate the dependence of the reactivity on cluster size, monodisperse gold nanoclusters (Au:PVP-*n*; *n* = 2–4) with average diameters up to ~5 nm were prepared by the seed-mediated growth method using Na<sub>2</sub>SO<sub>3</sub> as a reductant. Smaller cluster showed superior catalytic activity compared to larger clusters, suggesting that molecular oxygen species preferentially adsorbed on small Au clusters played an essential role in the formation of hydrogen peroxide.

### IX-N-2 Spectroscopic Investigation of Dendrimer-Encapsulated Gold Clusters

IMAMURA, Masaki<sup>1</sup>; MIYASHITA, Takeho<sup>1</sup>; TANAKA, Akinori<sup>1</sup>; YASUDA, Hidehiro<sup>1</sup>; YANAGIMOTO, Yasushi; NEGISHI, Yuichi; TSUKUDA, Tatsuya  
(<sup>1</sup>Kobe Univ.)

[*Trans. Mater. Res. Soc. Jpn.* **31**, 517–520 (2006)]

We have carried out the spectroscopic studies of dendrimer-encapsulated Au nanoclusters smaller than 2.4 nm. In this study, a 1.5th generation sodium carboxylate-terminated polyamidamine dendrimer was used as a template to control the size and stability of Au nanoclusters. The dendrimer-encapsulated Au nanoclusters were prepared by the chemical reduction of Au ions loaded within the dendrimer templates. The synthesized smallest nanocluster used in this work shows the

strong blue photoluminescence at 2.8 eV photon energy, while larger nanocluster shows no photoluminescence. Furthermore, we carried out the X-ray photoemission study in the valence-band region of dendrimer-encapsulated Au nanocluster. From these results, we will discuss the size dependent properties of Au nanoclusters encapsulated within the dendrimer templates.

### IX-N-3 Chromatographic Isolation of “Missing” Au<sub>55</sub> Clusters Protected by Alkanethiolates

TSUNOYAMA, Hironori; NEGISHI, Yuichi; TSUKUDA, Tatsuya

[*J. Am. Chem. Soc.* **128**, 6035–6037 (2006)]

We report on the first synthesis of alkanethiolate-protected Au<sub>55</sub> (11 kDa), which has been a “missing” counterpart of Schmid’s Au<sub>55</sub>(PR<sub>3</sub>)<sub>12</sub>Cl<sub>6</sub>. Au:SC<sub>x</sub> clusters (*x* = 12, 18) were prepared by the reaction of alkanethiol (C<sub>x</sub>SH) with polymer-stabilized Au clusters (~1.3 nm) and subsequently incubated in neat C<sub>x</sub>SH. The resulting clusters were successfully fractionated by recycling gel permeation chromatography into Au<sub>~38</sub>:SC<sub>x</sub> and Au<sub>~55</sub>:SC<sub>x</sub>, and identified by laser-desorption ionization mass spectrometry. The Au<sub>~55</sub>:SC<sub>x</sub> clusters exhibited structured optical spectra, suggesting molecular-like properties. The thiolate monolayers were found to be liquid-like on the basis of the IR spectrum and the monolayer thickness estimated from the hydrodynamic diameter.

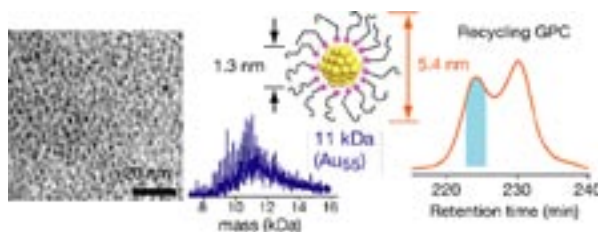


**Figure 1.** Isolation and characterization of Au<sub>55</sub>:SC<sub>x</sub>. [Reprinted with permission from *J. Am. Chem. Soc.* **128**, 6035–6037 (2006). Copyright (2006) American Chemical Society.]

### IX-N-4 Chiroptical Activity of BINAP-Stabilized Undecagold Clusters

YANAGIMOTO, Yasushi; NEGISHI, Yuichi;

FUJIHARA, Hisashi<sup>1</sup>; TSUKUDA, Tatsuya  
(<sup>1</sup>Kinki Univ.)

[*J. Phys. Chem. B* **110**, 11611–11614 (2006)]

Undecagold cluster compounds  $[\text{Au}_{11}(\text{BINAP})_4\text{X}_2]^+$  ( $\text{X} = \text{Cl}$  and  $\text{Br}$ ) were synthesized by chemical reduction of the corresponding precursor complexes,  $\text{Au}_2\text{X}_2$  (BINAP), where BINAP represents the bidentate phosphine ligand 2,2'-bis(diphenylphosphino)-1,1'-binaphthyl. The circular dichroism spectra of  $\text{Au}_{11}$  stabilized by the enantiomers  $\text{Au}_{11}(\text{R-BINAP})_4\text{X}_3$  and  $\text{Au}_{11}(\text{S-BINAP})_4\text{X}_3$  exhibited intense and mirror-image Cotton effect, whereas those of  $\text{Au}_{11}^{3+}$  clusters stabilized by achiral monodentate phosphine ligands did not. The origin of the chiroptical activity of  $[\text{Au}_{11}(\text{BINAP})_4\text{X}_2]^+$  is discussed in the context of the structural deformation of the  $\text{Au}_{11}^{3+}$  core.

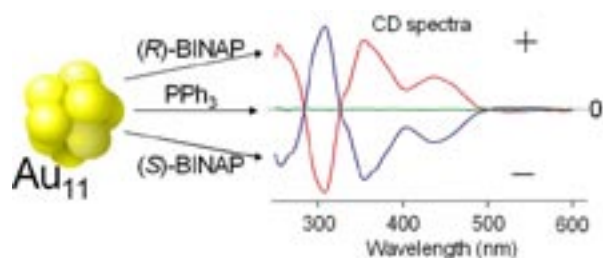


**Figure 1.** CD spectra of  $[\text{Au}_{11}(\text{BINAP})_4\text{X}_2]^+$ . [Reprinted with permission from *J. Phys. Chem. B* **110**, 11611–11614 (2006). Copyright (2006) American Chemical Society.]

#### IX-N-5 Kinetic Stabilization of Growing Gold Clusters by Passivation with Thiolates

NEGISHI, Yuichi; TAKASUGI, Yoshimitsu<sup>1</sup>; SATO, Seiichi<sup>1</sup>; YAO, Hiroshi<sup>1</sup>; KIMURA, Keisaku<sup>1</sup>; TSUKUDA, Tatsuya  
(<sup>1</sup>Univ. Hyogo)

[*J. Phys. Chem. B* **110**, 12218–12221 (2006)]

Small gold clusters (<1 nm), protected by monolayers of glutathione, *N*-(2-mercaptopropionyl)glycine or mercaptosuccinic acid, were prepared by reducing the corresponding Au(I)–thiolate polymers, and were fractionated by size using polyacrylamide gel electrophoresis (PAGE). Mass analysis of the fractionated clusters revealed that their core sizes varied with the molecular structures of the thiolates. This finding indicates that the reduction of the Au(I)–thiolate polymers yields small clusters whose growth is kinetically hindered by passivation with thiolates. Optical spectra of the clusters with identical compositions exhibited different profiles depending on the thiolate molecular structures, implying that deformation of the underlying gold cores is induced by inter-ligand interactions.

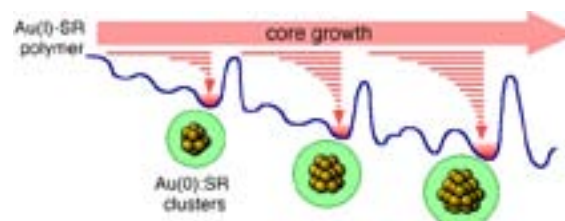


**Figure 1.** Kinetic stabilization of growing gold clusters by passivation with thiolates. [Reprinted with permission from *J. Phys. Chem. B* **110**, 12218–12221 (2006). Copyright (2006) American Chemical Society.]

#### IX-N-6 Size Effect on the Catalysis of Gold Clusters Dispersed in Water for Aerobic Oxidation of Alcohol

TSUNOYAMA, Hironori; SAKURAI, Hidehiro; TSUKUDA, Tatsuya

[*Chem. Phys. Lett.* **429**, 528–532 (2006)]

We prepared a set of nearly monodisperse gold clusters ranging from 1.3 to 10 nm by a seed-mediated growth in the presence of poly(*N*-vinyl-2-pyrrolidone) (PVP). The seed clusters with a diameter of  $1.3 \pm 0.3$  nm were prepared by reducing  $\text{AuCl}_4^-$  with  $\text{NaBH}_4$  in a low-temperature aqueous solution of PVP. Subsequent reduction of more  $\text{AuCl}_4^-$  by  $\text{Na}_2\text{SO}_3$  in the presence of the seed clusters yielded a series of larger Au:PVP clusters. Catalytic activities of the Au:PVP clusters for aerobic oxidation of *p*-hydroxybenzyl alcohol increased with decrease in the core size. The size dependence is discussed in light of the electronic structures of the cores probed by optical spectroscopy.

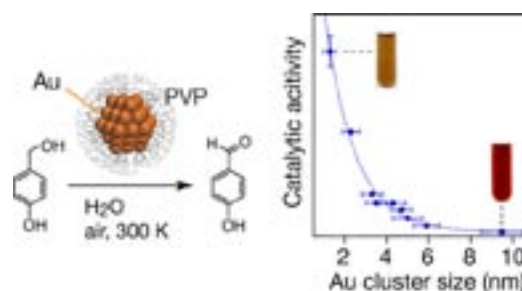


**Figure 1.** Catalytic activities of the Au:PVP clusters for aerobic oxidation of *p*-hydroxybenzyl alcohol increased with decrease in the core size. [Reprinted with permission from *Chem. Phys. Lett.* **429**, 528–532 (2006). Copyright (2006) Elsevier.]

#### IX-N-7 X-Ray Magnetic Circular Dichroism of Size-Selected, Thiolated Gold Clusters

NEGISHI, Yuichi; TSUNOYAMA, Hironori; SUZUKI, Motohiro<sup>1</sup>; KAWAMURA, Naomi<sup>1</sup>; MATSUSHITA, M. Michio<sup>2</sup>; MARUYAMA, Koichi; SUGAWARA, Tadashi<sup>2</sup>; YOKOYAMA, Toshihiko; TSUKUDA, Tatsuya  
(<sup>1</sup>JASRI/SPring-8; <sup>2</sup>Univ. Tokyo)

[*J. Am. Chem. Soc.* **128**, 12034–12035 (2006)]

We report herein the X-ray magnetic circular dichroism (XMCD) at the Au  $L_{2,3}$  edges of a series of Au clusters protected by glutathione (GSH). The samples used here included  $Au_N(SG)_M$  with  $(N, M) = (10, 10), (15, 13), (18, 14), (22, 16), (25, 18), (29, 20), (39, 24)$  and a sodium gold(I) thiomalate (SGT) as a reference. Magnetic moments per cluster were found to be increased with size, whereas those per Au–S bond were nearly constant. This finding suggests that a localized hole created by Au–S bonding at the gold/glutathione interface, rather than the quantum size effect, is responsible for the spin polarization of gold clusters.

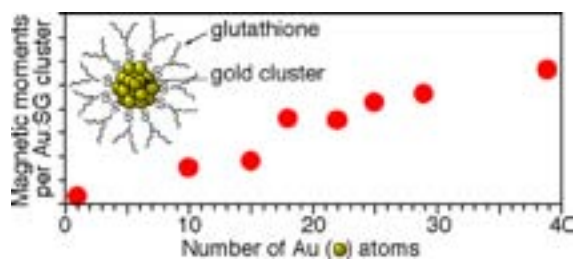


**Figure 1.** Magnetic moments per cluster as a function of core size.

[Reprinted with permission from *J. Am. Chem. Soc.* **128**, 12034–12035 (2006). Copyright (2006) American Chemical Society.]

#### IX-N-8 Mechanism of Selective Formation of Thiolated $Au_{25}$ Clusters in Ligand Exchange of Phosphine-Stabilized Gold Clusters: Size Focusing *via* Core Etching

SHICHIBU, Yukatsu; NEGISHI, Yuichi;  
TSUNOYAMA, Hironori; KANEHARA, Masayuki<sup>1</sup>;  
TERANISHI, Toshiharu<sup>1</sup>; TSUKUDA, Tatsuya  
(<sup>1</sup>Univ. Tsukuba)

Recently, we have succeeded in large-scale selective synthesis of  $Au_{25}:SG$  clusters *via* ligand exchange reactions of triphenylphosphine-stabilized  $Au_{11}$  clusters with glutathione (GSH) under optimized conditions (Shichibu, Y. *et al.* *J. Am. Chem. Soc.* **127**, 13464 (2005)). The mechanism of the selective formation of  $Au_{25}:SG$  was studied by monitoring the size distribution of the ligand exchange products using electrophoresis and optical absorption spectroscopy. It was found that the core size distributions of the  $Au_n:SG$  clusters extracted at the initial stage are polydisperse and are subsequently focused into  $Au_{25}:SG$  in the presence of free GSH molecules. The reaction of a series of the size-selected  $Au_n:SG$  clusters ( $n = 10, 15, 18, 22, 25, 29, 33, 39$ ) with free GSH under aerobic conditions revealed that two different reaction modes are operative depending on the core size. The  $Au_n:SG$  ( $n < 25$ ) clusters are completely oxidized to  $Au(I):SG$  complexes while  $Au_n:SG$  ( $n \geq 25$ ) clusters are etched into  $Au_{25}:SG$  by free GSH molecules. This indicates that the “ligand exchange reaction” we referred to in our previous paper, consists of two processes, *i.e.*, a ligand exchange accompanying rapid agglomeration of Au cores and subsequent etching of the cores. We conclude that the extremely high stability of  $Au_{25}:SG$  clusters against etching is the main cause for the selective formation.

Other gold clusters stabilized by polymer ( $\phi = 1.3 \pm 0.3$  nm) or triphenylphosphine ( $\phi = 1.5 \pm 0.4$  nm) were also converted selectively to  $Au_{25}:SG$  by treatment with excess GSH, supporting the proposed mechanism.

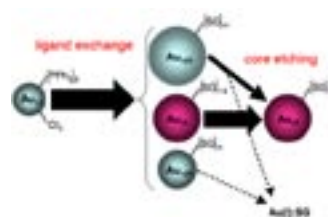


**Figure 1.** Mechanism of size focusing in the ligand exchange.

## IX-O Structural Analyses of Biological Macromolecules by Ultra-High Field NMR Spectroscopy

Our research seeks the underlying molecular basis for the function of biological macromolecules. In particular, we are interested in the function of molecular machines that work in the cellular processes involving protein folding, transport and degradation, and of glycoproteins playing important roles in the humoral and cellular immune systems. By use of ultra-high field NMR spectroscopy, we aim to elucidate the three-dimensional structure, dynamics, and interactions of proteins and glycoconjugates at the atomic level. Here we report stable-isotope-assisted NMR studies of Ufm1, a ubiquitin-like modifier, and IgG-Fc glycoprotein.

### IX-O-1 Solution Structure and Dynamics of Ufm1, a Ubiquitin-Fold Modifier 1

SASAKAWA, Hiroaki<sup>1</sup>; SAKATA, Eri<sup>2</sup>;  
YAMAGUCHI, Yoshiki<sup>1</sup>; KOMATSU, Masaaki<sup>3</sup>;  
TATSUMI, Kanako<sup>4</sup>; KOMINAMI, Eiki<sup>5</sup>; TANAKA,  
Keiji<sup>4</sup>; KATO, Koichi<sup>1</sup>

(<sup>1</sup>IMS and Nagoya City Univ.; <sup>2</sup>Nagoya City Univ.;  
<sup>3</sup>Tokyo Metropolitan Inst. Medical Sci. and Juntendo  
Univ.; <sup>4</sup>Tokyo Metropolitan Inst. Medical Sci.;  
<sup>5</sup>Juntendo Univ.)

[*Biochem. Biophys. Res. Commun.* **343**, 21–26 (2006)]

The ubiquitin-fold modifier 1 (Ufm1) is one of various ubiquitin-like modifiers and conjugates to target proteins in cells through Uba5 (E1) and Ufc1 (E2). The Ufm1-system is conserved in metazoa and plants, suggesting its potential roles in various multicellular organisms. Herein, we analyzed the solution structure and dynamics of human Ufm1 (hsUfm1) by nuclear magnetic resonance spectroscopy. Although the global fold of hsUfm1 is similar to those of ubiquitin (Ub) and NEDD8, the cluster of acidic residues conserved in Ub and NEDD8 does not exist on the Ufm1 surface. <sup>15</sup>N spin relaxation data revealed that the amino acid residues of hsUfm1 exhibiting conformational fluctuations form a cluster at the C-terminal segment and its spatial proximity, which correspond to the versatile ligand-binding sites of Ub and other ubiquitin-like proteins (Ubls). We suggest that Ub and other Ubl-modifiers share a common feature of potential conformational multiplicity, which might be associated with the broad ligand specificities of these proteins.

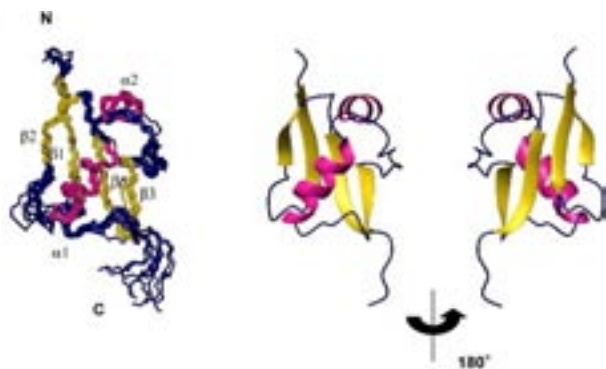


**Figure 1.** Backbone atom superposition of the final 10 structures (left) and ribbon representation of the lowest energy structure (right) of human Ufm1.

### IX-O-2 Glycoform-Dependent Conformational Alteration of the Fc Region of Human Immunoglobulin G1 as Revealed by NMR Spectroscopy

YAMAGUCHI, Yoshiki<sup>1</sup>; NISHIMURA, Mamiko<sup>2</sup>;  
NAGANO, Mayumi<sup>1</sup>; YAGI, Hirokazu<sup>1</sup>;  
SASAKAWA, Hiroaki<sup>1</sup>; UCHIDA, Kazuhisa<sup>3</sup>;  
SHITARA, Kenya<sup>3</sup>; KATO, Koichi<sup>1</sup>

(<sup>1</sup>IMS and Nagoya City Univ.; <sup>2</sup>Nagoya City Univ.;  
<sup>3</sup>Kyowa Hakko Kogyo Co., Ltd.)

[*Biochim. Biophys. Acta* **1760**, 693–700 (2006)]

The Fc portion of immunoglobulin G (IgG) expresses the biantennary complex type oligosaccharides at Asn297 of the C<sub>H</sub>2 domain of each heavy chain with microheterogeneities depending on physiological and pathological states. These N-glycans are known to be essential for promotion of proper effector functions of IgG such as complement activation and Fcγ receptor (FcγR)-mediated activities. To gain a better understanding of the role of Fc glycosylation, we prepared a series of truncated glycoforms of human IgG1-Fc and analyzed their interactions with human soluble FcγRIIIa (sFcγRIIIa) and with staphylococcal protein A by surface plasmon resonance and nuclear magnetic resonance (NMR) methods. Progressive but less pronounced reductions in the affinity for sFcγRIIIa were observed as a result of the galactosidase and subsequent N-acetylhexosaminidase treatments of IgG1-Fc. The following endoglycosidase D treatment, giving rise to a disaccharide structure composed of a fucosylated GlcNAc, abrogated the affinity of IgG1-Fc for sFcγRIIIa. On the other hand, those glycosidase treatments did not significantly affect the affinity of IgG1-Fc for protein A. Inspection of stable-isotope-assisted NMR data of a series of Fc glycoforms indicates that the stepwise trimming out of the carbohydrate residues results in concomitant increase in the number of amino acid residues perturbed thereby in the C<sub>H</sub>2 domains. Furthermore, the cleavage at the GlcNAcβ1-4GlcNAc glycosidic linkage induced the conformational alterations of part of the lower hinge region, which makes no direct contact with the carbohydrate moieties and forms the major FcγR-binding site, while the conformation of the C<sub>H</sub>2/C<sub>H</sub>3 interface was barely perturbed that is the protein A-binding site. These results indicate that the carbohydrate moieties are required for maintaining the structural integrity of the FcγR-binding site.

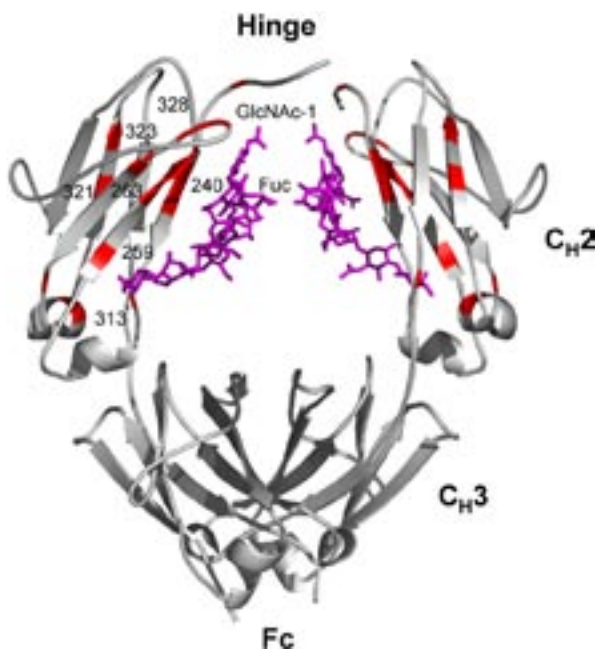


**Figure 1.** Mapping on the crystal structure of IgG1-Fc of the amino acid residues perturbed upon deglycosylation of carbohydrate chains attached onto Fc.